



Deriving Sensitivity Kernels of Coda-Wave Travel Times to Velocity Changes Based on the Three-Dimensional Single Isotropic Scattering Model

HISASHI NAKAHARA¹ and KENTARO EMOTO¹

Abstract—Recently, coda-wave interferometry has been used to monitor temporal changes in subsurface structures. Seismic velocity changes have been detected by coda-wave interferometry in association with large earthquakes and volcanic eruptions. To constrain the spatial extent of the velocity changes, spatial homogeneity is often assumed. However, it is important to locate the region of the velocity changes correctly to understand physical mechanisms causing them. In this paper, we are concerned with the sensitivity kernels relating travel times of coda waves to velocity changes. In previous studies, sensitivity kernels have been formulated for two-dimensional single scattering and multiple scattering, three-dimensional multiple scattering, and diffusion. In this paper, we formulate and derive analytical expressions of the sensitivity kernels for three-dimensional single-scattering case. These sensitivity kernels show two peaks at both source and receiver locations, which is similar to the previous studies using different scattering models. The two peaks are more pronounced for later lapse time. We validate our formulation by comparing it with finite-difference simulations of acoustic wave propagation. Our formulation enables us to evaluate the sensitivity kernels analytically, which is particularly useful for the analysis of body waves from deeper earthquakes.

Key words: Sensitivity kernel, coda waves, velocity change, single scattering.

1. Introduction

Coda-wave interferometry (e.g. Poupinet et al. 1984; Snieder et al. 2002) is a technique used to detect temporal changes in subsurface structures using coda waves from repeating natural earthquakes and/or active sources. Coda waves are very sensitive to subtle changes in material properties such as seismic velocity and attenuation, because they

propagate through a medium along long paths. The coda-wave interferometry technique has been used to detect seismic velocity changes associated with earthquakes (e.g. Poupinet et al. 1984; Nishimura et al. 2000) and volcanic eruptions (e.g. Ratdomopurbo and Poupinet 1995). In using such methods, it is often assumed that the spatial distribution of the velocity changes is uniform. This assumption is reasonable if we only want to know a spatial average of the velocity changes. In some cases when there is insufficient density of observation networks, a spatial average is all we can learn. Simplicity is another reason for the assumption of the spatial uniformity.

Localizing the spatial extent of velocity changes correctly is an important step toward the understanding of the physical mechanisms causing these changes. To develop coda-wave-based methods, which can localize such velocity changes, it is important to calculate sensitivity kernels of coda waves. The sensitivity kernels of coda-wave travel times show how a point-like slowness (or velocity) change affects the travel times of coda waves for a certain lapse time at a station. In this paper, we calculate sensitivity kernels for the case of single-scattering scalar waves in three dimensions (3D).

The first paper to have derived such sensitivity kernels is probably Pacheco and Snieder (2005) whose formulation is based on the diffusion model. The derived sensitivity kernels were found to have strong peaks at the source and the receiver locations. Later, formulations have been based on the single-scattering model of two-dimensional (2D) scalar waves (Pacheco and Snieder 2006) and the radiative transfer theory that includes the effect of multiple scattering for 3D (Maeda 2007) and 2D configurations (Obermann et al. 2013b). Recently, Margerin

¹ Department of Geophysics, Graduate School of Science, Tohoku University, 6-3, Aramaki-Aza-Aoba, Aoba-ku, Sendai 980-8578, Japan. E-mail: naka@zisin.gp.tohoku.ac.jp

et al. (2016) succeeded in including the effect of anisotropic scattering using radiative transfer theory. A 3D single scattering of scalar waves has not yet been formulated as far as we know, even though 3D configurations are suitable for body waves. Hence, we make this formulation and try to validate it with numerical simulations.

The sensitivity kernels are used in practice. Larose et al. (2010) developed a technique called LOCADIFF, which succeeded in detecting a weak change in a medium from active acoustic experiment data. Rossetto et al. (2011) showed that LOCADIFF exploited the sensitivity kernels of coda-wave decoherence (i.e. loss of coherence) to weak medium changes which were derived based on a diffusion model. Regarding ambient noise tomography (e.g. Shapiro et al. 2005), Hobiger et al. (2012) introduced a simplified version of the sensitivity kernel of coda-wave travel times which has non-zero value only at the source and the receiver and neglects contributions from the rest of the regions. Obermann et al. (2013a) formulated linear inverse problems to estimate the locations of changes in seismic velocity as well as seismic scattering from changes in travel times and decoherence of the coda of ambient noise cross-correlations using the strict sensitivity kernels based on radiative transfer theory. They detected precursory changes associated with eruptions in October and December, 2010 at Piton de la Fournaise volcano in Reunion Island. We expect that our formulation of coda-wave sensitivity based on 3D single-scattering model will also contribute to ambient noise tomography.

2. Formulation

We formulate the sensitivity kernels of coda-wave travel times to slowness changes (or velocity changes) based on the 3D scalar single isotropic scattering model. This is an extension of the 2D configurations studied by Pacheco and Snieder (2006) to the 3D configurations. A setup of our model is shown in Fig. 1. A source, a receiver, a region of velocity change, and a scatterer are shown by a solid star, a solid triangle, a solid square, and a solid circle, respectively. Note that the source, the receiver, the

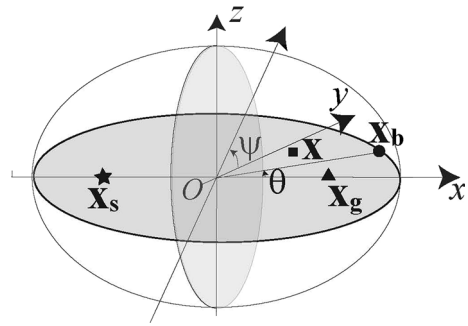


Figure 1

Setup of a model. A source, a receiver, a point of velocity change, and a scatterer are shown by a solid star, a solid triangle, a solid square, and a solid circle, respectively. These four points are all located on an ellipse marked with dark gray. An isochronal scattering shell composes a spheroid

region of velocity change, and the scatterer are all situated on a single ellipse shaded by dark gray. Because only the single scattering is considered, coda waves arriving at the receiver at a certain lapse time are composed of scattered waves coming from the scatterers on an isochronal scattering shell (a spheroid in 3D cases).

2.1. Definition of the Sensitivity Kernel

Pacheco and Snieder (2006) derived the following relation for $\langle \delta t \rangle(t)$, the expected travel time change of coda waves at a lapse time of t for a source at \mathbf{x}_s and a receiver at \mathbf{x}_g due to a slowness change $\delta S(\mathbf{x})$ at a point \mathbf{x} :

$$\begin{aligned} \langle \delta t \rangle(t) &= \int_V K(\mathbf{x}_s, \mathbf{x}_g, \mathbf{x}, t) \delta S(\mathbf{x}) dV(\mathbf{x}) \\ &= - \int_V K(\mathbf{x}_s, \mathbf{x}_g, \mathbf{x}, t) \frac{\delta v(\mathbf{x})}{v(\mathbf{x})^2} dV(\mathbf{x}), \quad (1) \end{aligned}$$

where $K(\mathbf{x}_s, \mathbf{x}_g, \mathbf{x}, t)$ is the sensitivity kernel, $S(\mathbf{x})$ is the slowness that is the reciprocal of velocity $v(\mathbf{x})$, and dV is the infinitesimal volume element. $\langle \rangle$ means ensemble average with respect to realizations of medium heterogeneities. The sensitivity kernel $K(\mathbf{x}_s, \mathbf{x}_g, \mathbf{x}, t)$ is expressed by the contributions of single-scattering paths crossing the point of velocity changes among all the single-scattering paths reaching the receiver at a lapse time t . This kernel is represented by energy density calculated based on the

single-scattering model. Under the single-scattering assumption, the number of the single-scattering paths crossing the point of velocity change is only two, as shown in Fig. 2. The first path shown by a solid line is named path-s and passes through the point of the velocity change at \mathbf{x} on the way from the source to the scatterer at \mathbf{x}_{bs} . The other path shown by a dotted line is named path-g, and goes through the point of the change at \mathbf{x} on the way from the scatterer at \mathbf{x}_{bg} to the receiver. Therefore, we need to calculate energy densities for the two paths based on the 3D scalar single isotropic scattering model (e.g. Sato 1977).

2.2. Formulation of Travel Time Changes of Coda Waves

In the following formulation, we refer to the coordinate system shown in Fig. 3. Travel time along a single-scattering path lp is expressed as:

$$t_p = \int_{lp} s_0 dl = \int_{lp} \frac{dl}{v_0} = \int_{ls} \frac{dl}{v_0} + \int_{lg} \frac{dl}{v_0} = \frac{r_s + r_g}{v_0}, \tag{2}$$

where ls is a segment of the path from the source to a scatterer, lg is the other segment of the path from the scatterer to the receiver, r_s is the distance between the source and the scatterer at \mathbf{x}_b and r_g is the distance between the scatterer at \mathbf{x}_b and the receiver, dl is the

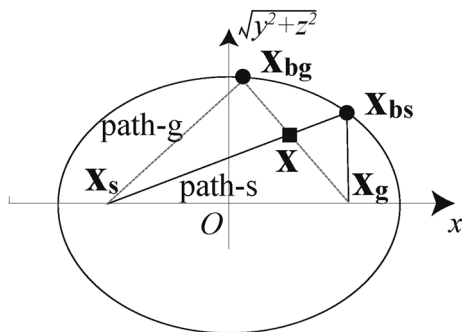


Figure 2

An elliptical coordinate on which a source, a receiver, a point of velocity change, and scatterers are located. An ellipse shows the isochronal scattering shell for the single scattering. There are only two paths of the single scattering that go through a point of velocity change at \mathbf{x} . One path that crosses \mathbf{x} between the source at \mathbf{x}_s and the scatterer at \mathbf{x}_{bs} is denoted as path-s, and the other path that crosses \mathbf{x} between the scatterer at \mathbf{x}_{bg} and the receiver at \mathbf{x}_g is denoted as path-g

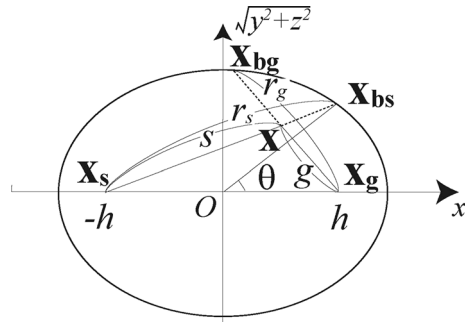


Figure 3

An elliptical coordinate on which a source, a receiver, a point of velocity change, and scatterers are located

line element along each path, s_0 is the slowness at point \mathbf{x} on the path, and v_0 is the velocity at the same point. If a slowness change $\delta S(\mathbf{x})$ is assumed to be small, the path lp is the same as before the slowness change. Hence, the corresponding travel time change is approximately:

$$\delta t_p \approx \int_{lp} \delta S(\mathbf{x}) dl(\mathbf{x}). \tag{3}$$

According to Pacheco and Snieder (2006), the following relations can be derived:

$$\langle \delta t \rangle(t) = \frac{\int dV(\mathbf{x}_b) \{ \delta t_s(\mathbf{x}) + \delta t_g(\mathbf{x}) \} w(\mathbf{x}_b, t)}{\int dV(\mathbf{x}_b) w(\mathbf{x}_b, t)}. \tag{4}$$

Here, δt_s and δt_g are travel time changes along ls and lg , respectively. This relation holds for 3D, too. We explicitly show that the volume integral should be with respect to the scatterer location \mathbf{x}_b , which is different from the notation in Pacheco and Snieder (2006). The single-scattering energy density that is radiated from a unit-amplitude source and is scattered at \mathbf{x}_b on the scattering shell in a 3D medium having a spatially uniform scattering coefficient g_0 is represented as:

$$w(x_b, t) = \frac{g_0}{r_s^2 r_g^2} \delta \left(t - \frac{r_s + r_g}{v_0} \right). \tag{5}$$

This is different from the 2D case. Note that the geometrical spreading is proportional to the reciprocal of the squared distance and the delta function means that energy propagates with a velocity v_0 . Substitution of Eq. (5) into Eq. (4) gives:

$$\begin{aligned}
\langle \delta t \rangle(t) = & \frac{\int_V dV(\mathbf{x}_{bs}) \int_{ls(\mathbf{x}_{bs})} \delta S(\mathbf{x}) d\mathbf{l}(\mathbf{x}) \frac{g_0}{r_s^2 r_g^2} \delta \left(t - \frac{r_s + r_g}{v_0} \right)}{\int_V dV(\mathbf{x}_b) \frac{g_0}{r_s^2 r_g^2} \delta \left(t - \frac{r_s + r_g}{v_0} \right)} \\
& + \frac{\int_V dV(\mathbf{x}_{bg}) \int_{lg(\mathbf{x}_{bg})} \delta S(\mathbf{x}) d\mathbf{l}(\mathbf{x}) \frac{g_0}{r_s^2 r_g^2} \delta \left(t - \frac{r_s + r_g}{v_0} \right)}{\int_V dV(\mathbf{x}_b) \frac{g_0}{r_s^2 r_g^2} \delta \left(t - \frac{r_s + r_g}{v_0} \right)}. \quad (6)
\end{aligned}$$

This equation expresses how the coda-wave travel time changes with slowness changes. The denominator is the energy density of all single-scattered energy with lapse time t . The first term and the second term are the contributions of the two segments ls and lg , respectively. For the path- s , the travel time change occurs along ls but not along lg , because lg does not cross the region of velocity change. We specify the scatterer location at \mathbf{x}_{bs} for the path- s . Similarly, for the path- g , the travel time change occurs along lg but not along ls , and the corresponding scatterer location is at \mathbf{x}_{bg} .

2.3. Evaluation of the Terms

We evaluate all the terms in (6). For the purpose, we use a prolate spheroidal coordinate as shown in Fig. 1 (e.g. Morse and Feshbach 1953; Sato et al. 2012) for which the following relations hold:

$$\begin{aligned}
x_b &= h\varepsilon \cos \theta, \\
y_b &= h\sqrt{\varepsilon^2 - 1} \sin \theta \cos \psi, \\
z_b &= h\sqrt{\varepsilon^2 - 1} \sin \theta \sin \psi,
\end{aligned} \quad (7)$$

where h is the half-length between source and receiver.

$$\varepsilon = \frac{r_s + r_g}{2h} \quad (8)$$

$$\cos \theta = \frac{r_s - r_g}{2h}. \quad (9)$$

The coordinate variables take the following range: $\varepsilon \geq 1$, $0 \leq \theta \leq \pi$, $0 \leq \psi < 2\pi$.

It is necessary to distinguish between the location of the scatterer \mathbf{x}_b and that of the velocity change \mathbf{x} . In Eq. (7), we use a suffix b to mean the scatterer

location. The infinitesimal volume element dV at the scatterer location \mathbf{x}_b is expressed using the Jacobian:

$$\begin{aligned}
dV(\mathbf{x}_b) &= \left| \frac{\partial(x, y, z)}{\partial(\varepsilon, \theta, \psi)} \right| d\varepsilon d\theta d\psi \\
&= h^3 \sin \theta (\varepsilon^2 - \cos^2 \theta) d\varepsilon d\theta d\psi = \sqrt{y^2 + z^2} dA d\psi. \quad (10)
\end{aligned}$$

The term in the denominator that is proportional to the single-scattered energy density at a lapse time of t can be calculated by the method of Sato (1977) as follows:

$$\begin{aligned}
I_D &= \int_V dV(\mathbf{x}_b) \frac{1}{r_s^2 r_g^2} \delta \left(t - \frac{r_s + r_g}{v_0} \right) = \frac{\pi}{h^2} v_0 \int_0^\pi d\theta \frac{\sin \theta}{\left(\frac{v_0 t}{2h} \right)^2 - \cos^2 \theta} \\
&= \frac{\pi v_0}{h^2} \frac{1}{2h} \log \left| \frac{1 + \frac{v_0 t}{2h}}{1 - \frac{v_0 t}{2h}} \right| = \frac{\pi v_0}{h^2} K_s \left(\frac{v_0 t}{2h} \right), \quad (11)
\end{aligned}$$

where K_s is the K function in Sato (1977). In the course of the calculation, the following two relations are used:

$$\delta(v_0 t - (r_s + r_g)) = \delta(v_0 t - 2h\varepsilon) = \frac{1}{2h} \delta \left(\varepsilon - \frac{v_0 t}{2h} \right), \quad (12)$$

$$r_s r_g = h(\varepsilon - \cos \theta)h(\varepsilon + \cos \theta) = h^2(\varepsilon^2 - \cos^2 \theta). \quad (13)$$

Equation (12) restricts the contribution only from a spheroidal scattering shell. Substitution of Eqs. (10)–(13) into Eq. (6) leads to:

$$\begin{aligned}
\langle \delta t \rangle(t) &= \frac{1}{I_D} \frac{v_0}{2h^2} \int_0^{2\pi} d\psi \int_0^\pi d\theta \int_1^\infty d\varepsilon \frac{\sin \theta}{\varepsilon^2 - \cos^2 \theta} \\
&\quad \times \left[\int_{ls} \delta \left(\varepsilon - \frac{v_0 t}{2h} \right) \delta S(\mathbf{x}) d\mathbf{l}(\mathbf{x}) + \int_{lg} \delta \left(\varepsilon - \frac{v_0 t}{2h} \right) \delta S(\mathbf{x}) d\mathbf{l}(\mathbf{x}) \right]. \quad (14)
\end{aligned}$$

We deal with the first term in the numerator that corresponds to ls for the path- s :

$$\begin{aligned}
I_s &= \frac{v_0}{2h^2} \int_0^{2\pi} d\psi \int_0^\pi d\theta \int_1^\infty d\varepsilon \frac{\sin \theta}{\varepsilon^2 - \cos^2 \theta} \left[\int_{ls} \delta \left(\varepsilon - \frac{v_0 t}{2h} \right) \delta S(\mathbf{x}) d\mathbf{l}(\mathbf{x}) \right] \\
&= \frac{v_0}{2h^2} \int_0^{2\pi} d\psi \int_0^\pi d\theta \frac{\sin \theta}{\left(\frac{v_0 t}{2h} \right)^2 - \cos^2 \theta} \left[\int_{ls} \delta S(\mathbf{x}) d\mathbf{l}(\mathbf{x}) \right] \quad (15)
\end{aligned}$$

and the second term corresponding to lg for the path-g:

$$\begin{aligned}
 I_g &= \frac{v_0}{2h^2} \int_0^{2\pi} d\psi \int_0^\pi d\theta \int_1^\infty d\varepsilon \frac{\sin \theta}{\varepsilon^2 - \cos^2 \theta} \left[\int_{lg} \delta(\varepsilon - \frac{v_0 t}{2h}) \delta S(\mathbf{x}) dV(\mathbf{x}) \right] \\
 &= \frac{v_0}{2h^2} \int_0^{2\pi} d\psi \int_0^\pi d\theta \frac{\sin \theta}{\left(\frac{v_0 t}{2h}\right)^2 - \cos^2 \theta} \left[\int_{lg} \delta S(\mathbf{x}) dV(\mathbf{x}) \right].
 \end{aligned}
 \tag{16}$$

Finally, we need to use the infinitesimal volume element $dV(\mathbf{x})$ at the point of velocity change \mathbf{x} , not at the point of the scatter \mathbf{x}_b , in terms of θ , ψ , and l . This is possible as shown in Appendix. Then, we obtain:

$$\begin{aligned}
 \frac{I_s}{I_D} &= \frac{1}{2\pi h^2 \left\{ \left(\frac{v_0 t}{2h}\right)^2 - 1 \right\}} \frac{1}{\left[\frac{2h}{v_0 t} \log \left| \frac{1 + \frac{v_0 t}{2h}}{1 - \frac{v_0 t}{2h}} \right| \right]} \\
 &\times \int \frac{r_s}{s} \frac{1}{\left(\frac{v_0 t}{2h}\right)^2 - \left(\frac{2x_{bs}}{v_0 t}\right)^2} \delta S(\mathbf{x}) dV(\mathbf{x}).
 \end{aligned}
 \tag{17}$$

Here, note that x_{bs} appears which denotes x -coordinate of the scatterer for the segment ls of the path- s . Repeating a similar calculation for the remaining segment lg of the path- g gives:

$$\begin{aligned}
 \frac{I_g}{I_D} &= \frac{1}{2\pi h^2 \left\{ \left(\frac{v_0 t}{2h}\right)^2 - 1 \right\}} \frac{1}{\left[\frac{2h}{v_0 t} \log \left| \frac{1 + \frac{v_0 t}{2h}}{1 - \frac{v_0 t}{2h}} \right| \right]} \\
 &\times \int \frac{r_g}{g} \frac{1}{\left(\frac{v_0 t}{2h}\right)^2 - \left(\frac{2x_{bg}}{v_0 t}\right)^2} \delta S(\mathbf{x}) dV(\mathbf{x}).
 \end{aligned}
 \tag{18}$$

Here, x_{bg} is x -coordinate of the scatterer for the segment lg of the path- g . Using the relation of

$$\langle \delta t \rangle(t) = \frac{I_s + I_g}{I_D} \equiv \int_V K(\mathbf{x}_s, \mathbf{x}_g, \mathbf{x}, t) \delta S(\mathbf{x}) dV(\mathbf{x}),
 \tag{19}$$

we can finally derive the kernel as:

$$\begin{aligned}
 K(\mathbf{x}_s, \mathbf{x}_g, \mathbf{x}, t) &= \frac{1}{2\pi h^2 \left\{ \left(\frac{v_0 t}{2h}\right)^2 - 1 \right\}} \frac{1}{\left[\frac{2h}{v_0 t} \log \left| \frac{1 + \frac{v_0 t}{2h}}{1 - \frac{v_0 t}{2h}} \right| \right]} \\
 &\times \left\{ \frac{\frac{r_s}{s}}{\left(\frac{v_0 t}{2h}\right)^2 - \left(\frac{2x_{bs}}{v_0 t}\right)^2} + \frac{\frac{r_g}{g}}{\left(\frac{v_0 t}{2h}\right)^2 - \left(\frac{2x_{bg}}{v_0 t}\right)^2} \right\}.
 \end{aligned}
 \tag{20}$$

This is an analytical expression. Once we give h , v_0 , t , and (x, y, z) , we can calculate s , g , r_s , r_g , x_{bs} , x_{bg} , and, accordingly, the kernel K . More details are described in the next section.

3. Practical Calculation of the Sensitivity Kernels

Here, we calculate the sensitivity kernels for some specific cases and try to see their characteristics.

3.1. Steps for Calculating the Sensitivity Kernels

First, we mention the steps needed to calculate the sensitivity kernels. For the calculation, we take the following steps:

1. Assume a velocity of scalar waves v_0 .
2. Locate the source and receiver by providing h . We also need to specify the lag time of coda waves t .
3. Specify the location of velocity change \mathbf{x} .
4. Calculate s and g as:

$$s = \sqrt{(x+h)^2 + y^2 + z^2}, \quad g = \sqrt{(x-h)^2 + y^2 + z^2}.
 \tag{21}$$

5. Deal with only the points of velocity change within a corresponding scattering shell:

$$1 \leq \frac{s+g}{2h} \leq \frac{v_0 t}{2h}.
 \tag{22}$$

6. Calculate r_s and r_g as follows:

$$r_s = h \frac{\left(\frac{v_0 t}{2h}\right)^2 - 1}{\frac{v_0 t}{2h} - \frac{x+h}{s}}, \quad r_g = h \frac{\left(\frac{v_0 t}{2h}\right)^2 - 1}{\frac{v_0 t}{2h} - \frac{-x+h}{g}}.
 \tag{23}$$

7. Calculate x_{bs} and x_{bg} as follows:

$$x_{bs} = \frac{r_s}{s}(x+h) - h, \quad x_{bg} = \frac{r_g}{g}(x-h) + h.
 \tag{24}$$

8. Evaluate the sensitivity kernel for the given \mathbf{x} .
9. Repeat the steps of 3–8 for all points of velocity change within the scattering shell to calculate the expected travel time changes due to the slowness changes (or velocity changes) given.

3.2. Calculation of the Sensitivity Kernels

Following the steps described in the previous subsection, we are able to calculate the sensitivity

kernels of coda-wave travel times. In Fig. 4, we show two results for the case of $h = 1000$ m, $v_0 = 6000$ m/s, and the lapse times of (a) 0.5 s and (b) 1 s. Here, we also assume $z = 0$ in the calculation. The problem is axially symmetric about the x -axis thanks to isotropic scattering and the spatial homogeneity of the medium. The sensitivity has non-zero values within the corresponding single-scattering isochronal shell. The region of the isochronal scattering shell is found to become wider for later lapse times. Two strong peaks exist at the source and the receiver. This is mainly due to the fact that all the paths must go through the source and the receiver. We also notice that the peaks are smaller in comparison to the remaining regions for (a) an earlier lapse time than for (b) a later lapse time. In short, the peaks are more pronounced for later lapse times. This is probably because the contribution of the two single-scattering paths crossing points of velocity change, except at the source and receiver, becomes smaller for later lapse times.

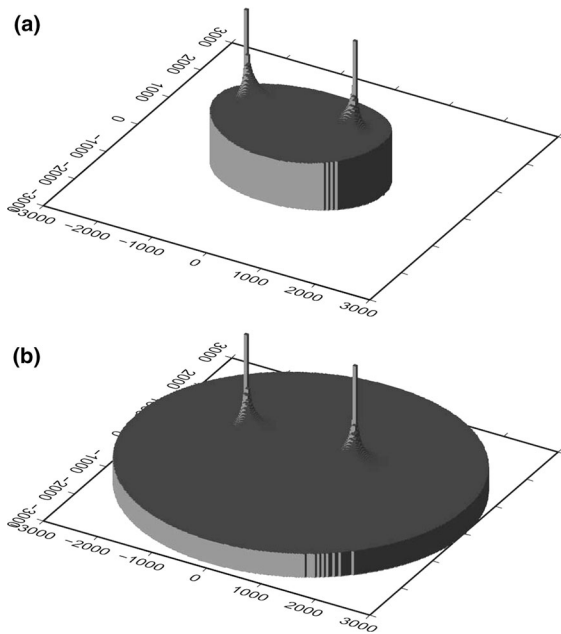


Figure 4

Two examples of the sensitivity kernels for $h = 1000$ m, $v_0 = 6000$ m/s, and the lapse time of **a** 0.5 s and **b** 1 s. Amplitudes of the sensitivity kernels are shown in logarithmic scale

4. Discussions

4.1. Comparison of the Sensitivity Kernels Between 3D and 2D

Here, we consider the effect of dimensionality on the sensitivity kernels. We compare the sensitivity kernels for 3D cases with those for 2D cases. The sensitivity kernels were derived by Pacheco and Snieder (2006) based on the 2D scalar single isotropic scattering model as follows:

$$K(\mathbf{x}_s, \mathbf{x}_g, \mathbf{x}, t) = \frac{1}{2\pi h \sqrt{\left(\frac{v_0 t}{2h}\right)^2 - 1}} \left(\frac{r_s}{s} + \frac{r_g}{g} \right) \quad (25)$$

Figure 5 shows the sensitivity kernel for 3D case (a) and 2D case (b) with the assumed parameters of $h = 1000$ m, $v_0 = 6000$ m/s, and $t = 0.5$ s. Similar to Fig. 4, the resolution kernel has non-zero values within the scattering shell with two remarkable peaks at the source and the receiver. Comparing the 3D case with the 2D case, we find that the peaks are more pronounced for 3D case than 2D case. This is

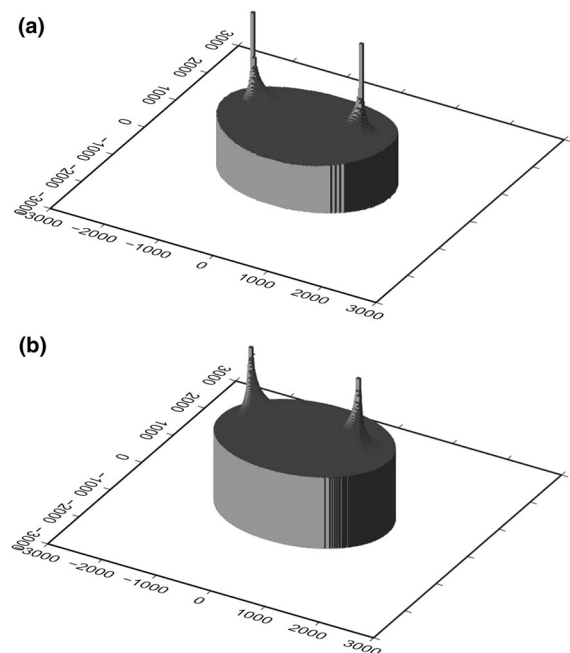


Figure 5

Comparison of the sensitivity kernels between **a** 3D and **b** 2D. $h = 1000$ m, $v_0 = 6000$ m/s, and the lapse time of 0.5 s for both cases. Amplitudes of the sensitivity kernels are shown in logarithmic scale

probably due to the fact that the two single-scattering paths become rarer for 3D cases than 2D cases. This difference is due to dimensionality.

4.2. Validation of the Formulation with Finite-Difference Simulations of Acoustic Wave Propagation

We have formulated the sensitivity kernels of coda-wave travel times due to velocity changes based on the assumptions of the single scattering, isotropic source radiation, and isotropic scattering. It is necessary to check the validity of our derivations by comparing with finite-difference simulations of strict 3D acoustic wave propagation in heterogeneous media. The validation of the analytical derivations with finite-difference simulations was conducted for 2D case by Pacheco and Snieder (2006).

For the acoustic simulations, we synthesize waveforms with a finite-difference algorithm with the accuracy of the fourth-order in space and the second-order in time. Configuration of the simulation is shown in Fig. 6. Background velocity structure is assumed to have a random fluctuation of $e = 2\%$ around an average of $v_0 = 6000$ m/s obeying an exponential auto-correlation function with the correlation length $a = 40$ m. The slowness perturbation of 0.5% (velocity perturbation of -0.5%) is given in a cuboid shown by black. Spatial grid intervals are 10 m in all three perpendicular directions. The number of grids are $3600 \times 3328 \times 3328$. All the

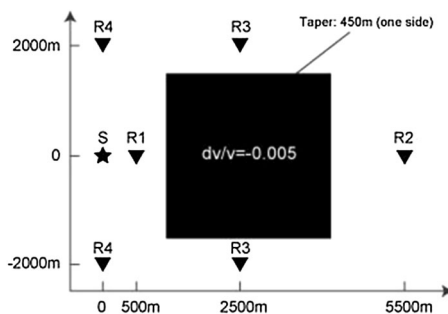


Figure 6

Configuration of finite-difference simulation of acoustic wave propagation in a 3D random medium. Background velocity structure is assumed to have random fluctuations around an average velocity. The slowness perturbation of 0.5% (velocity change of -0.5%) is provided in the *black cuboid*. A *solid star* marks a source and *solid triangles* mark receivers

boundaries are reflecting ones. A source time function at the source is the Kupper wavelet with the duration of 28 ms. The simulation is performed up to 5 s with a time step of 0.7 ms. The mean free time that is the average time for one scattering to take place is estimated to be about 16.7 s by $a/(e^2 v_0)$. The lapse time range of up to 5 s in our numerical simulations is smaller than the mean free time of 16.7 s, which supports the predominance of the single scattering. The wavelength for a frequency of 20 Hz is 300 m, that is about ten times larger than the correlation length of $a = 40$ m. For this case, an isotropic scattering is predicted to dominate according to the Born approximation (e.g. Sato et al. 2012). To achieve effective large-scale simulations, a domain partitioning technique using the message passing interface is employed after Furumura and Chen (2004). We try five different realizations of the random velocity fluctuation by changing random number seeds. Four receivers (R1, R2, R3, and R4) are set in the medium. Regarding R3 and R4, we consider that four points are identical thanks to the geometrical symmetry around x -axis, which practically increases the number of realizations.

In the top panels of Fig. 7, simulated waveforms at two receivers R1 and R2 are shown on the left and the right, respectively, for a realization of the random media. In the bottom panels, simulated waveforms in the lapse times of 1.5–1.7 s are zoomed up. In each panel, a gray solid curve shows a waveform for an unperturbed medium and a black one is for a perturbed medium. Because a slower perturbation is provided, the black curves for the perturbed medium lag behind the gray curves for the unperturbed medium. Using the cross-spectral moving window technique (e.g. Poupinet et al. 1984), travel time changes of coda waves for the perturbed waveforms due to the slowness perturbation are measured with respect to those for the unperturbed waveforms. The time window for the calculation has a length of 0.4 s and is shifted with a time step of 0.2 s. The travel time change is measured by the slope of phase spectrum with respect to frequency in 10–30 Hz. The results are shown by symbols in the top panel of Fig. 8. Different symbols mean different realizations. We also plot the expected travel time changes based on our analytical formulation with red solid curves.

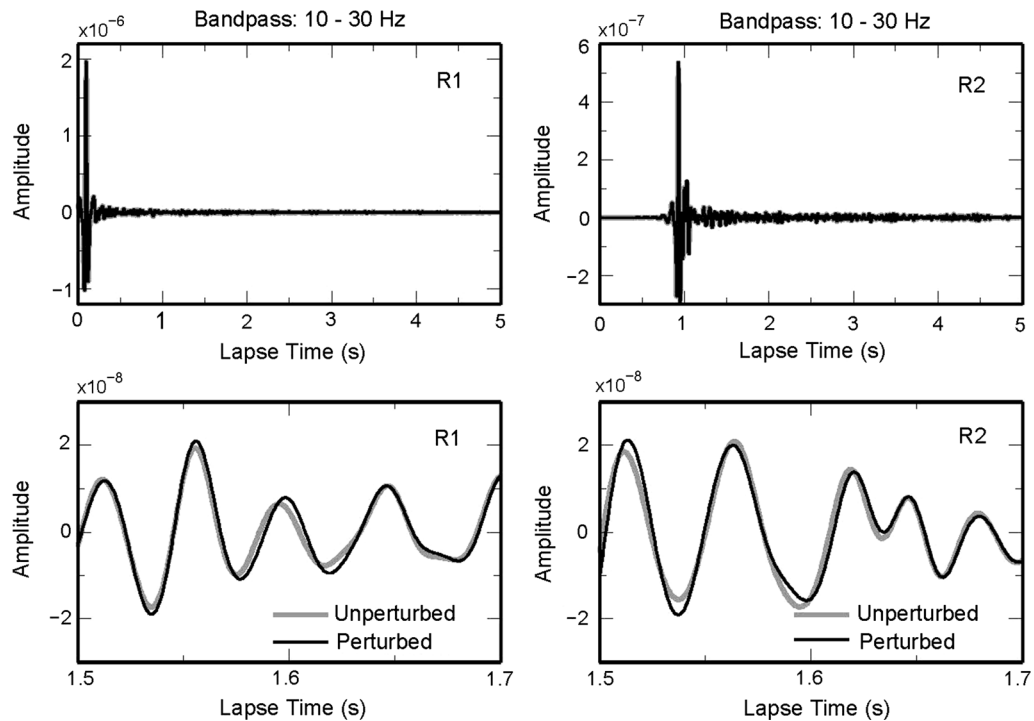


Figure 7

Simulated waveforms at receivers R1 and R2 are shown in *left and right panels*, respectively. *Top panels* show waveforms in the lapse time between 0 and 5 s and *bottom panels* show those between 1.5 and 1.7 s. A *gray solid curve* shows a waveform for an unperturbed medium and a *black one* is for a perturbed medium

Matches are not so good for the direct wave part but improve for coda wave parts though some underestimation seems to occur in the theoretical expectations. Indeed, we notice that the matches between numerical simulations and our formulations are good for receivers R4 and R1. However, for receiver R2, the direct wave appearing at the lapse time of about 0.917 s is delayed by 0.0025 s because the velocity decreases by 0.5 % over 3000 m along the ray path. Though numerical simulations reproduce this delay well, our theoretical formulation predicts a delay of about 0.0015 s and clearly underestimates. Similar underestimation occurs for receiver R3 where the direct wave is expected to delay by about 0.0008 s. Though reasons why the underestimation of the travel time change is significant only for the receivers R2 and R3 are not fully understood, we point out that the path of the direct wave does cross the region of velocity change for the

two receivers. Because the direct wave is not included in our formulation, we speculate that the direct wave has some effect on the underestimation. We conclude that our formulation is better for coda waves especially at stations where the path of the direct wave does not cross the region of velocity change.

In our theoretical formulation, we only consider single-scattered waves. Though it is possible to include the direct waves, we would need to know the scattering coefficient to calculate the sensitivity kernels. In our formulation, we deal with infinite space without any boundaries. A free surface is better to be considered. However, the inclusion of a free surface in the modeling would hamper analytical derivations. Moreover, to consider more realistic structural complexities like layering, topography, multiple scattering, and so on, it is necessary to resort to finite-difference numerical simulations. For example, Kanu and Snieder

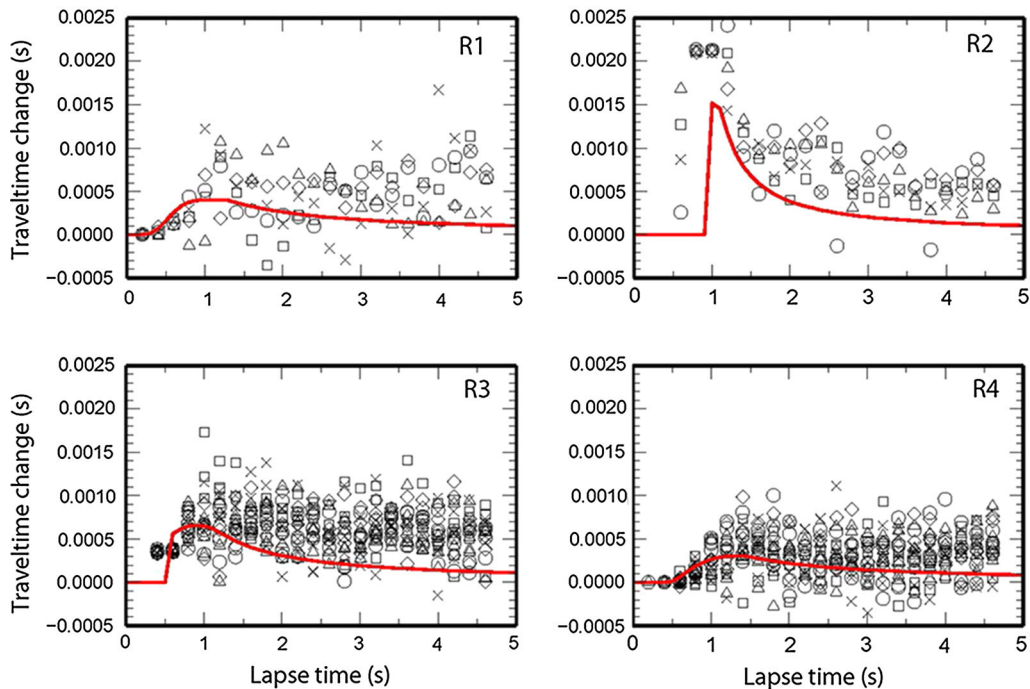


Figure 8

Travel time changes of coda waves of the perturbed waveforms due to the slowness perturbation with respect to the unperturbed waveforms at four receivers of R1, R2, R3, and R4. *Open circles, open triangles, open squares, crosses, and open diamonds* are measured by applying the cross-spectral moving window technique (e.g. Poupinet et al. 1984) to the waveforms calculated by the finite-difference simulation for different realizations of random media. Theoretical travel time changes based on our formulation are shown by *red solid curves*

(2015) calculated the sensitivity kernels for the multiple scattering regime in 2D layered structures.

5. Conclusions

We have formulated the sensitivity kernels of coda-wave travel times to slowness perturbation (or velocity perturbation) based on the 3D scalar single isotropic scattering model. The derived kernels can be expressed analytically. The kernels show two strong peaks at the source and the receiver, because all the paths must go through the source and receiver. The peaks are more pronounced for later coda. Comparing with finite-difference simulations, the kernels derived in this study are found to underestimate around direct wave arrivals because they are not included in the formulation. But the kernels are better for coda waves. The sensitivity kernels derived in this study will be helpful when dealing with coda waves comprising body waves especially from deeper earthquakes.

Acknowledgments

This study was supported by Grant-in-Aid for Scientific Research (C) (16K05528) from Japan Society for the Promotion of Science (JSPS) and the Ministry of Education, Culture, Sports, Science and Technology (MEXT). Computations were conducted on the Earth Simulator at the Japan Agency for Marine-Earth Science and Technology (JAMSTEC) under the support of a joint research project between Earthquake Research Institute, the University of Tokyo, and Center of Earth Information Science and Technology entitled “Numerical simulations of seismic- and tsunami-wave propagation in 3D heterogeneous earth”.

Appendix

We show how to evaluate the infinitesimal volume element in the prolate spheroidal coordinate shown in Fig. 9. We extend 2D configuration of

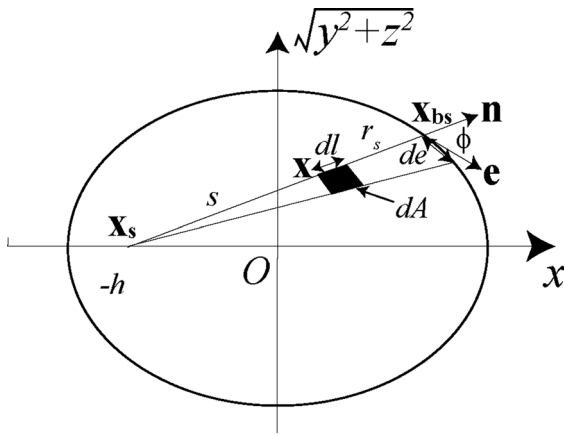


Figure 9

An elliptical coordinate on which a source, a receiver, a point of velocity change, and a scatterer are located for calculating the infinitesimal areal element dA

Pacheco and Snieder (2006) to 3D configuration. The infinitesimal areal element dA at \mathbf{x} (a point of velocity change) is expressed as:

$$dA(\mathbf{x}) = dlde \frac{s}{r_s} \sin \phi. \quad (26)$$

Here, de is defined along a spheroidal scattering shell and calculated as:

$$\begin{aligned} de &= \sqrt{\left(\frac{\partial x_{bs}}{\partial \theta}\right)^2 + \left(\frac{\partial y_{bs}}{\partial \theta}\right)^2 + \left(\frac{\partial z_{bs}}{\partial \theta}\right)^2} d\theta \\ &= h\sqrt{\varepsilon^2 \sin^2 \theta + (\varepsilon^2 - 1) \cos^2 \theta} d\theta \\ &= h\sqrt{\varepsilon^2 - \cos^2 \theta} d\theta = h\sqrt{\left(\frac{v_0 t}{2h}\right)^2 - \cos^2 \theta} d\theta. \end{aligned} \quad (27)$$

Note that $\mathbf{x}_{bs} = (x_{bs}, y_{bs}, z_{bs})$ is the location of a scatterer on the scattering shell for the path ls . In the derivation, the following relations are used:

$$\begin{aligned} \frac{\partial x_{bs}}{\partial \theta} &= \frac{\partial}{\partial \theta} (h\varepsilon \cos \theta) = -h\varepsilon \sin \theta, \\ \frac{\partial y_{bs}}{\partial \theta} &= \frac{\partial}{\partial \theta} (h\sqrt{\varepsilon^2 - 1} \sin \theta \cos \psi) = h\sqrt{\varepsilon^2 - 1} \cos \theta \cos \psi, \\ \frac{\partial z_{bs}}{\partial \theta} &= \frac{\partial}{\partial \theta} (h\sqrt{\varepsilon^2 - 1} \sin \theta \sin \psi) = h\sqrt{\varepsilon^2 - 1} \cos \theta \sin \psi. \end{aligned} \quad (28)$$

The unit vector \mathbf{n} directing away from the source along the path ls is:

$$\begin{aligned} \mathbf{n} &= \frac{1}{\sqrt{(h + x_{bs})^2 + y_{bs}^2 + z_{bs}^2}} \begin{pmatrix} h + x_{bs} \\ y_{bs} \\ z_{bs} \end{pmatrix} \\ &= \frac{1}{\varepsilon + \cos \theta} \begin{pmatrix} \varepsilon \cos \theta + 1 \\ \sqrt{\varepsilon^2 - 1} \sin \theta \cos \psi \\ \sqrt{\varepsilon^2 - 1} \sin \theta \sin \psi \end{pmatrix}. \end{aligned} \quad (29)$$

The unit vector \mathbf{e} directing along the edge of the ellipse is:

$$\begin{aligned} \mathbf{e} &= \frac{1}{\sqrt{\left(\frac{\partial x_{bs}}{\partial \theta}\right)^2 + \left(\frac{\partial y_{bs}}{\partial \theta}\right)^2 + \left(\frac{\partial z_{bs}}{\partial \theta}\right)^2}} \begin{pmatrix} \frac{\partial x_{bs}}{\partial \theta} \\ \frac{\partial y_{bs}}{\partial \theta} \\ \frac{\partial z_{bs}}{\partial \theta} \end{pmatrix} \\ &= \frac{1}{\sqrt{\varepsilon^2 - \cos^2 \theta}} \begin{pmatrix} -\varepsilon \sin \theta \\ \sqrt{\varepsilon^2 - 1} \cos \theta \cos \psi \\ \sqrt{\varepsilon^2 - 1} \cos \theta \sin \psi \end{pmatrix}. \end{aligned} \quad (30)$$

The term of $\sin \phi$ can be calculated using the vector product between \mathbf{n} and \mathbf{e} as:

$$\sin \phi = |\mathbf{n} \times \mathbf{e}| = \frac{\sqrt{\varepsilon^2 - 1}}{\sqrt{\varepsilon^2 - \cos^2 \theta}} = \frac{\sqrt{\left(\frac{v_0 t}{2h}\right)^2 - 1}}{\sqrt{\left(\frac{v_0 t}{2h}\right)^2 - \cos^2 \theta}}. \quad (31)$$

Equations (26), (27), (31), (7) and (10) give the volume element dV at \mathbf{x} as:

$$dV(\mathbf{x}) = h^2 \left\{ \left(\frac{v_0 t}{2h}\right)^2 - 1 \right\} \frac{s}{r_s} \sin \theta d\theta d\psi. \quad (32)$$

REFERENCES

- Furumura, T., & Chen, L. (2004). Large scale parallel simulation and visualization of 3-D seismic wavefield using Earth simulator. *Computer Modeling in Engineering and Sciences*, 6, 153–168.
- Hobiger, M., Wegler, U., Shiomi, K., & Nakahara, H. (2012). Coseismic and postseismic elastic wave velocity variations caused by the 2008 Iwate-Miyagi Nairiku earthquake, Japan. *Journal Geophysical Research*, 117, B09313. doi:10.1029/2012jb009402.
- Kanu, C., & Snieder, R. (2015). Time-lapse imaging of a localized weak change with multiply scattered waves using numerical-based sensitivity kernel. *Journal Geophysical Research*, 120, 5595–5605. doi:10.1002/2015JB011871.
- Larose, E., Planes, T., Rossetto, V., & Margerin, L. (2010). Locating a small change in a multiple scattering environment. *Applied Physics Letters*, 96(20), 204101. doi:10.1063/1.3431269.
- Maeda, T. (2007). Sensitivity kernel of coda envelopes (in Japanese). Paper Presented at the Seismic Scattering Workshop.

- University of Tokyo, Tokyo, 25–26 September 2007, <http://www.eic.eri.u-tokyo.ac.jp/viewdoc/scat2007/14-maeda.pdf>.
- Margerin, L., Planes, T., Mayol, J., & Calvet, M. (2016). Sensitivity kernels for coda-wave interferometry and scattering tomography: theory and numerical evaluation in two-dimensional anisotropically scattering media. *Geophysical Journal International*, 204, 650–666.
- Morse, P. M., & Feshbach, H. (1953). *Methods of theoretical physics* (Vol. I). New York: McGraw-Hill.
- Nishimura, T., Uchida, N., Sato, H., Ohtake, M., Tanaka, S., & Hamaguchi, H. (2000). Temporal changes of the crustal structure associated with the M6.1 earthquake on September 3, 1998, and the volcanic activity of Mount Iwate, Japan. *Geophysical Research Letters*, 27(2), 269–272.
- Obermann, A., Planes, T., Larose, E., & Campillo, M. (2013a). Imaging preruptive and coeruptive structural and mechanical changes of a volcano with ambient seismic noise. *Journal Geophysical Research*, 118, 6285–6294.
- Obermann, A., Planes, T., Larose, E., Sens-Schonfelder, C., & Campillo, M. (2013b). Depth sensitivity of seismic coda waves to velocity perturbations in an elastic heterogeneous medium. *Geophysical Journal International*, 194(1), 372–382.
- Pacheco, C., & Snieder, R. (2005). Time-lapse travel time change of multiply scattered acoustic waves. *Journal of the Acoustic Society of America*, 118(3), 1300–1310.
- Pacheco, C., & Snieder, R. (2006). Time-lapse traveltime change of singly scattered acoustic waves. *Geophysical Journal International*, 165(2), 485–500.
- Poupinet, G., Ellsworth, W. L., & Frechet, J. (1984). Monitoring velocity variations in the crust using earthquake doublets—An application to the Calaveras fault, California. *Journal Geophysical Research*, 89, 5719–5731.
- Ratdomopurbo, A., & Poupinet, G. (1995). Monitoring a temporal change of seismic velocity in a volcano—Application to the 1992 eruption of Mt-Merapi (Indonesia). *Geophysical Research Letters*, 22(7), 775–778.
- Rossetto, V., Margerin, L., Planes, T., & Larose, E. (2011). Locating a weak change using diffuse waves: Theoretical approach and inversion procedure. *Journal of Applied Physics*, 109(3), 034903. doi:10.1063/1.3544503.
- Sato, H. (1977). Energy propagation including scattering effect: Single isotropic scattering approximation. *Journal of Physics of the Earth*, 25, 27–41.
- Sato, H., Fehler, M. C., & Maeda, T. (2012). *Seismic wave propagation and scattering in the heterogeneous earth* (2nd ed.). Berlin: Springer.
- Shapiro, N. M., Campillo, M., Stehly, L., & Ritzwoller, M. H. (2005). High-resolution surface-wave tomography from ambient seismic noise. *Science*, 307, 1615–1618.
- Snieder, R., Gret, A., Douma, H., & Scales, J. (2002). Coda wave interferometry for estimating nonlinear behavior in seismic velocity. *Science*, 295(5563), 2253–2255.

(Received February 10, 2016, revised July 1, 2016, accepted July 18, 2016, Published online August 5, 2016)